

Fabrication of Microfluidic Channels by Femtosecond Laser Micromachining and Application in Optofluidics

João M. Maia^{1,2}, Vítor A. Amorim^{1,2}, D. Alexandre^{2,3} and P. V. S. Marques^{1,2}

¹*Department of Physics and Astronomy of Faculty of Sciences, University of Porto,*

Rua do Campo Alegre 687, Porto, Portugal

²*CAP – Centre for Applied Photonics, INESC TEC, Rua Dr. Roberto Frias, Porto, Portugal*

³*Department of Physics of School of Science and Technology, University of Trás-os-Montes e Alto Douro, Quinta de Prados 5000-801, Vila Real, Portugal*

Keywords: Optofluidics, Femtosecond Laser Direct Writing, Micromachining, Chemical Etching, Fused Silica.

Abstract: Micromachining with femtosecond laser can be exploited to fabricate optical components and microfluidic channels in fused silica, due to internal modification of the glass properties that is induced by the laser beam. In this paper, we refer to the formation of microfluidic channels, where an optimization of the fabrication procedure was conducted by examining etch rate and surface roughness as a function of the irradiation conditions. Microfluidic channels with high and uniform aspect ratio and with smooth sidewalls were obtained, and such structures were successfully integrated with optical components. The obtained results set the foundations towards the development of new optofluidic devices.

1 INTRODUCTION

The concept of lab-on-a-chip (LOC) revolves around the idea of miniaturizing a complete laboratory into a hand-sized chip, which allows preparation, transport, reaction and analysis of reagents, without loss of efficiency and measurement accuracy (Dittrich, 1996).

These devices integrate multiple systems, such as microfluidic channels (for fluid movement), mechanical elements (valves and mixers for control of reagent flow and reaction (Xu, 2013, Liu, 2013)) and optical elements (mirrors, lenses and waveguides for in situ analysis (Hwang, 2009)).

Although conventional fabrication techniques, such as photolithography and soft lithography, enabled production of microfluidic devices (Vos, 2007, Wu, 2004), some problems remain. First, both techniques are planar, thus hindering fabrication of three-dimensional (3D) structures and limiting integration of components and device functionalities. Second, integration of microfluidic systems with optical layers for on-chip optical detection has been proven to be demanding and complex.

In order to overcome these issues, femtosecond laser micromachining has been adopted for the production of LOC devices. This non-contact technology relies on the laser ability to internally modify the sample properties, due to a non-linear absorption process (Osellame, 2012). The modification is confined to the focal volume, hence submicron resolutions are attainable. Given the ultrashort duration of the laser pulse, the modification is not a result of thermal diffusion, thus formation of heat-affected zones is minimized (Sugioka, 2014). In the case of picosecond pulses the resulting structures are formed due to cumulative thermal effects, which result in erratic and irregular structures (Corbari, 2013).

For ultrashort pulses, the laser-matter interaction can be described qualitatively in three steps: (i) generation of free electron plasma, (ii) followed by energy relaxation and (iii) modification of the material properties. When fused silica is exposed to a femtosecond laser beam, two important structural modifications may occur, depending on the pulse energy. For low energies, there is a smooth modification of the refractive index that can be exploited to produce optical waveguides, Bragg grating waveguides, directional couplers, among other devices (Zeil, 2013, Davis, 1996). For

moderate energies, birefringent sub-wavelength nanogratings are formed. These structures are more selective to an etching reaction, which allows fabrication of microfluidic channels.

Although these two effects may be combined to produce optofluidic devices (Bellini, 2010, Applegate, 2006), some problems regarding reactant detection are still unsolved. As the size of the microfluidic systems decrease, so does detection volume, usually in the range of 10^{-9} to 10^{-12} litres, and surface-to-volume ratio, hence surface forces (surface tension, van der Waals and surface roughness) become dominant (Stone, 2004). Therefore, the fabrication procedure of microfluidic channels needs to be optimized, in order to form highly sensitive optofluidic systems.

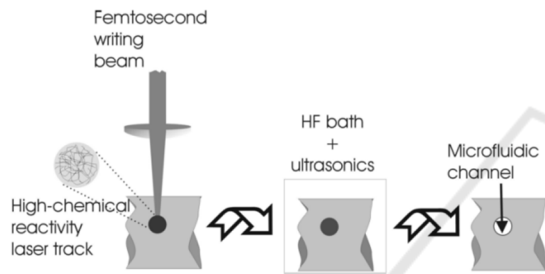


Figure 1: Illustration of the FLICE fabrication technique in fused silica (Said, 2004).

2 MICROFLUIDIC CHANNEL FABRICATION PROCEDURE

The microfluidic channels were produced using the FLICE technique (Femtosecond Laser Irradiation followed by Chemical Etching), which is depicted in figure 1.

To machine fused silica, we use the 2nd harmonic (515 nm) of a fiber-amplified laser from Amplitude Systèmes. The laser has a pulse duration of 250 fs at repetition rate of 500 kHz and maximum average energy of 1.1 μ J. A schematic of the laser direct writing unit is depicted in figure 2.

The first block is a power control unit, which is followed by a beam expander system formed by two planar-convex lenses. This expander increases the beam spot size so that it equals the objective lens entrance aperture. The beam polarization is determined by a half-wave plate.

The laser beam is focused inside the sample by an aspherical objective lens with 40x amplification and numerical aperture equal to 0.55, which prevents spherical aberrations.

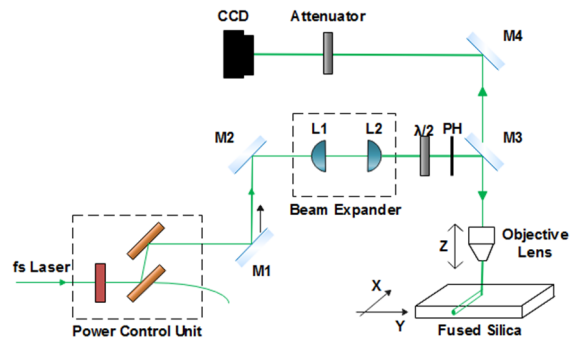


Figure 2: Laser direct writing unit.

The objective is mounted in a piezoelectric stage (PI P-725) that moves along Z, while the sample is mounted in two air-bearing stages (Aerotech ABL10100-LN) that move along the plane XY. This way we can write 3D structures, by defining the design geometry in a software program that controls stage position, speed and pulse energy.

The channels were written by focusing the beam inside the glass and by stacking multiple scans side by side, starting from below (in order to avoid beam propagation through areas already exposed). This strategy allows design of different cross-section geometries to be obtained.

After writing, the sample edges were polished to enable cross-section characterization by microscopy. Then, the etching reaction was performed by immersion of the sample in a 10% hydrofluoric acid (HF) solution. The reaction was performed in an ultrasonic bath (Branson 2510 Ultrasonic Cleaner) at frequency of 40 kHz to facilitate debris removal.

After etching the samples were rinsed in isopropanol and then in deionized water. The samples were characterized by direct observation at an optical microscope and by performing SEM microscopy.

3 OPTIMIZATION OF FABRICATION PARAMETERS

The production of microfluidic channels was optimized by studying two main parameters: etch rate and surface roughness. The etch rate is associated with the etching selectivity that should be high, and with the aspect ratio (length/cross-section) which should be uniform. The channel should also present smooth sidewalls (low surface roughness), to enable light coupling and to minimize optical losses due to scattering.

Multiple channels were fabricated while varying beam polarization (parallel or perpendicular to the scanning direction), pulse energy (60 nJ to 300 nJ), scanning speed (100 $\mu\text{m/s}$ to 500 $\mu\text{m/s}$), scanning depth (50 μm to 150 μm) and scan separation (1 μm to 15 μm).

3.1 Etch Rate Calibration

We started by analyzing the etch rate dependence on the polarization angle. The results, shown in figure 3, indicate a strong dependence on the polarization angle, which results from the nanogratings orientation.

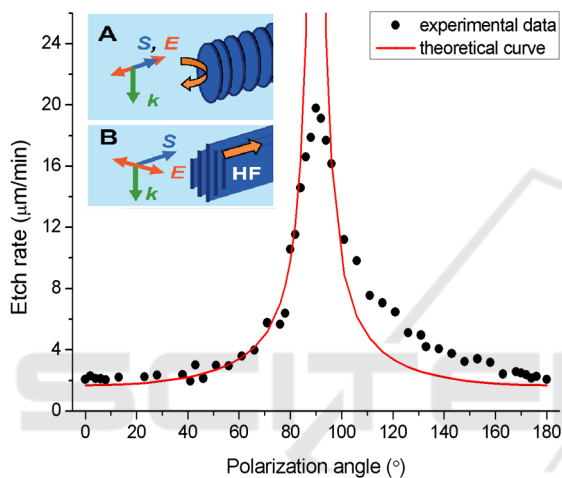


Figure 3: Etch rate vs polarization angle of single-scan channels fabricated 150 μm below surface at 500 $\mu\text{m/s}$ and with 80 nJ pulse energy. The figure inset shows the nanograting orientation for writing with (A) parallel polarization and (B) perpendicular polarization, alongside the light propagation direction (k), the writing direction (S), and the laser electric field vector (E) (Taylor, 2008).

For perpendicular polarization (90°), the etch rate is maximum, because the nanogratings align with the channel axis, enabling fast HF diffusion. For parallel polarization (0° and 180°), the planes are normal to the writing direction, hence the HF acid encounters alternate layers of nanogratings and pristine material, which reduce the etch rate. To take advantage of a maximum etch rate, we then decided to write the channels with perpendicular polarization.

Analyzing the influence of pulse energy and scanning speed, figure 4, we observed that, within the tested range, the etch rate stays uniform. We also determined that at pulse energies lower than 60 nJ, there is no formation of nanogratings, and hence there is no etching selectivity. For scanning speeds

higher than 500 $\mu\text{m/s}$, we expect the etch rate to start decreasing, due to a lower contrast between nanogratings and pristine volumes.

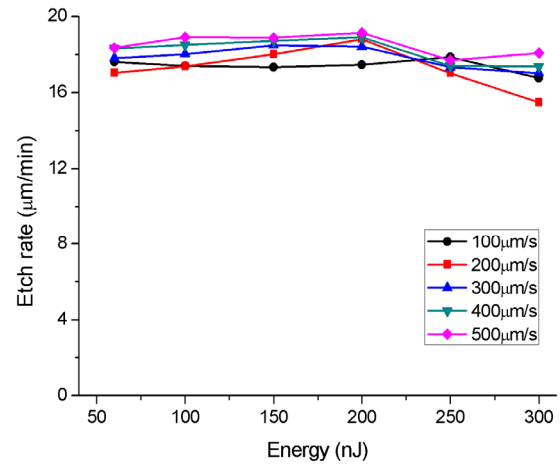


Figure 4: Etch rate as a function of the pulse energy and scanning speed for channels fabricated with perpendicular polarization and 150 μm below the silica surface.

The etch rate also depends on the separation between scans. As shown in figure 5, the etch rate starts increasing as the separation between scans decreases, as expected.

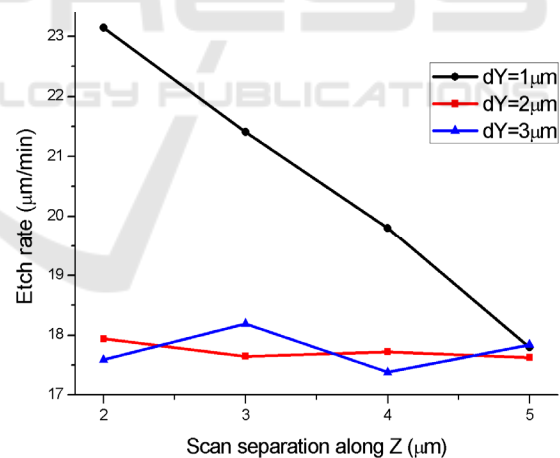


Figure 5: Etch rate of channels as function of the separation between scans along Y and Z. The channels were fabricated with perpendicular polarization, 150 μm below surface at 500 $\mu\text{m/s}$ and with pulse energy of 80nJ.

For small overlap, the scans do not interact with each other and the etch rate is similar to the one obtained for single-scan channels. However, decreasing the separation results in an increase of the stress field around the laser-affected zones (Champion, 2013), which modifies the irradiated

volume density, and consequently increases the etch rate (Agarwal, 1997).

3.2 Tapering Effect

For long etching reactions we also observed that, for writing with perpendicular polarization, the etch rate decreases over time, figure 6. This phenomenon occurs because the HF acid cannot reach the channel's end as easily.

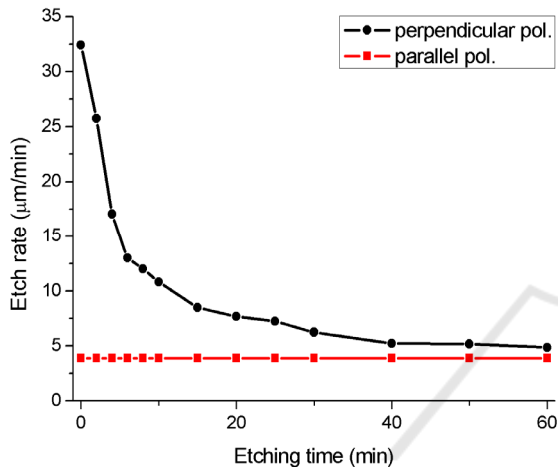


Figure 6: Etch rate as a function of the etching reaction time for channels written with perpendicular and parallel polarization. The channels written with perpendicular polarization were fabricated 150 μm below surface at 500 $\mu\text{m/s}$ and with pulse energy of 80nJ. The channels written with parallel polarization were fabricated 150 μm below surface at 300 $\mu\text{m/s}$ and with pulse energy of 300 nJ. For perpendicular polarization the etch rate decreases over time, while for parallel polarization it remains constant.

Alongside this effect, it also occurs lateral etching, where the HF acid etches the pristine material surrounding the channel. These two features contribute to the formation of tapered channels, figure 7, and affect significantly the obtained aspect ratio.

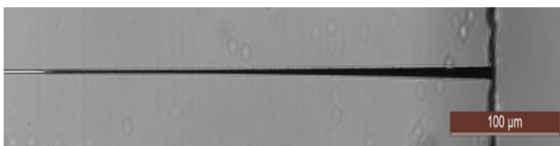


Figure 7: Top view image of a tapered single-scan channel fabricated with perpendicular polarization at a depth of 50 μm , with pulse energy of 60 nJ and scanning speed of 500 $\mu\text{m/s}$.

In order to prevent this issue, several solutions can be adopted: (i) use of KOH at 80°C as an etchant solution (Kiyama, 2009), (ii) design of a structure that compensates and balances the etching reaction (Vishnubhatla, 2009), and (iii) fabrication of vertical holes connecting the channel to the sample surface (Ho, 2013). Due to simplicity, we used the latter technique, whose configuration is depicted in figure 8.

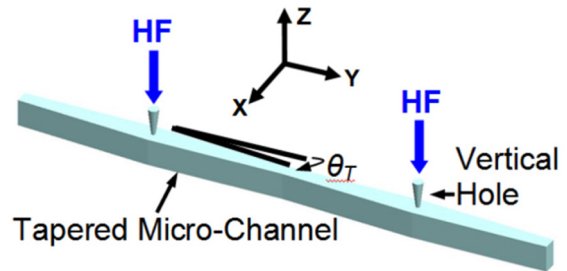


Figure 8: Fabrication layout of vertical holes (Ho, 2013).

By fabricating holes 200 μm apart from each other, we obtained channels with uniform aspect ratio, as shown in figure 9, and with length over one centimetre.

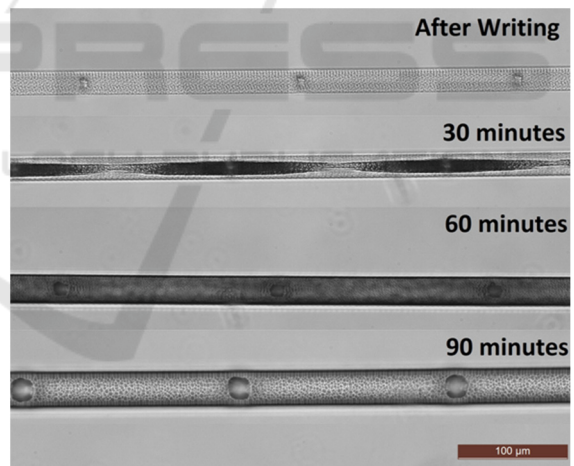


Figure 9: Top view images of microfluidic channels fabricated buried in fused silica at different times of etching reaction.

Figure 9 also reveals the time evolution of the etching reaction. After 30 minutes, we observe that the vertical holes have been fully etched, and that the HF acid diffuses preferentially along the channel axis, due to the favourable nanogratings alignment. After 60 minutes, the entire channel has been etched, but its dark colour reveals that some glass fibers are still present. After 90 minutes the process is completed.

3.3 Surface Roughness

Regarding surface roughness, it depends mainly on two factors: stress field distribution and scan separation.

The formation of laser-affected zones is associated with the generation of stress fields around the irradiated volume. The stress fields induce birefringence, which can be measured by transmitting light through the sample.

It is reported that pulse energy, scan separation and beam polarization affect the accumulated stress (Champion, 2013). For high pulse energies and for small separations the accumulated stress increases, and at extreme conditions (pulse energy above 300 nJ and/or separation of tenths of nanometres) the stress can be released. This relaxation process generates cracks that propagate over a few microns into the surroundings, figure 10.

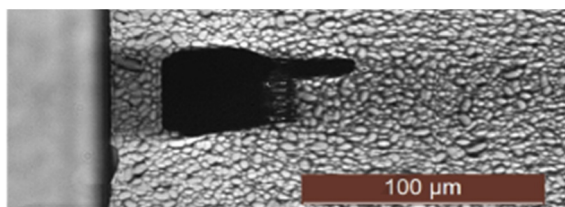


Figure 10: Cross-section image of a microfluidic channel presenting cracks. The channel was fabricated with parallel polarization, 50 μm below surface at 200 $\mu\text{m}/\text{s}$ and with 300nJ pulse energy.

On the other hand, if the laser-affected zones are separated by tenths of microns, we observe that, after etching, these volumes do not merge together, figure 11. By decreasing the scan separation, the volumes start merging, but the sidewalls are still strongly corrugated. Therefore, it is necessary to continue decreasing the scan separation to obtain smoother sidewalls, while avoiding, at the same time, crack formation.

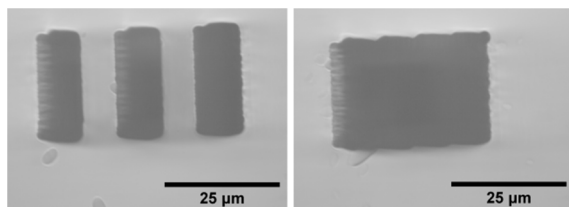


Figure 11: Cross-section image of microfluidic channels fabricated with different scan separations along Y and Z: 1 μm and 15 μm (left) and 1 μm and 7 μm (right), respectively. Both channels were fabricated with perpendicular polarization, 150 μm below surface at 500 $\mu\text{m}/\text{s}$ and with 80 nJ pulse energy.

3.4 Optimum Conditions

From this study, we found that the optimum irradiation conditions to obtain long channels with uniform aspect ratio and smooth sidewalls are: beam polarization perpendicular to the scanning direction (to obtain maximum etching selectivity), scanning speed of 500 $\mu\text{m}/\text{s}$, pulse energy between 60 nJ and 80 nJ (to minimize stress accumulation), scan separation along Y of 1 μm to 2 μm and along Z of 1 μm to 4 μm and scanning depth between 50 μm and 150 μm .

Under these conditions, we obtained a maximum etching selectivity of 140:1.

The surface roughness along Y varied between 100 nm and 200 nm. This value was obtained by producing the channels at the silica surface and by measuring the roughness using a profilometer (Dektak XT from Bruker with stylus with 2 μm radius and with 3 mg applied force). Regarding surface roughness along Z we estimate it to be of tenths of nanometres, given that similar values were obtained by other groups who produced channels under identical conditions (Ho, 2013). In addition, it is expected that the surface roughness is lower along Z than along Y due to the parallel alignment of the nanogratings with the channel sidewalls.

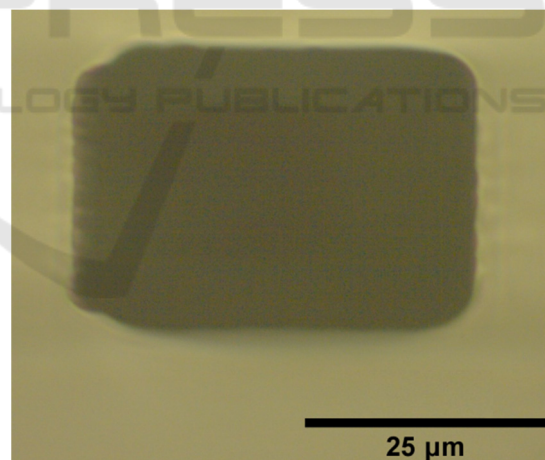


Figure 12: Cross-section of a microfluidic channel fabricated under optimum conditions.

4 ON-CHIP OPTICAL DETECTION

4.1 Principle of Operation

The results presented in the previous section indicate that the obtained channels may be integrated with

optical components for production of optofluidic devices. In this paper, we present a possible on-chip optical detection scheme that enables measurement of refractive index and temperature of the fluid circulating in the channel.

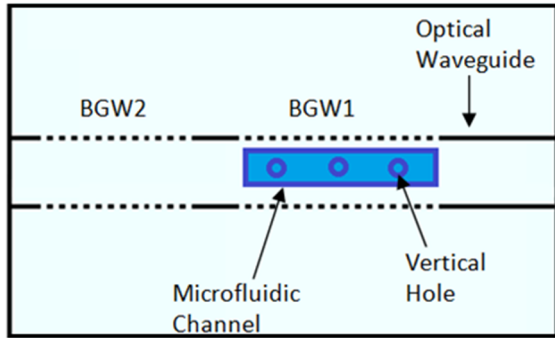


Figure 13: Optical detection scheme layout.

The proposed scheme, whose layout is shown in figure 13, consists in placing a Bragg grating waveguide (BGW1) a few microns from the microfluidic channel. According to the Bragg law, equation (1), light being reflected by the BGW depends on the medium effective index (n_{eff}).

$$\lambda_B = 2\Lambda n_{eff} \quad (1)$$

If the channel is a few microns from the BGW, the medium effective index will depend on the fluid present in the channel. Therefore, by changing the fluid properties (concentration, temperature) or by changing the fluid, we obtain a different Bragg wavelength (λ_B) and are able to sense the fluid properties. A second BGW, which is surrounded only by pristine, is fabricated with a different modulation period (Λ) and is designed to serve as reference, allowing to exclude thermal effects.

4.2 Proof of Concept

We started by fabricating microfluidic channels with BGWs at increasing distances from the channel.

The channels were 1.1 cm long and 100 μm below the glass surface (distance between silica surface and top of the channel), and were fabricated with perpendicular polarization, at 500 $\mu\text{m/s}$ with 60 nJ pulse energy and with scan separation along Y and Z equal to 1 μm and 2 μm , respectively. The Bragg grating waveguides were produced with parallel polarization, 125 μm below surface at 400 $\mu\text{m/s}$ and with 250 nJ pulse energy. Two gratings were produced, one to sense the channel and designed to operate at 1550 nm and another to operate at 1558 nm and to serve as a reference. After

writing, the glass facets were polished to improve light coupling. The etching reaction lasted 90 minutes.

After the devices were fabricated, we observed at an optical microscope that some of the BGWs had been etched, figure 14, suggesting that a higher control of the etching reaction is needed.



Figure 14: Top view of the optofluidic device.

Regarding the remaining devices, we characterized them, by measuring the Bragg wavelength when the channels were filled with air. The measurements were performed without polarization control. The results, shown in table 1, indicate that the wavelength shift decreases as the BGW-channel separation increases. Thus, we conclude that to achieve higher sensitivities the gap should be, at maximum, 5 μm .

Table 1: Wavelength shift for increasing separation between BGW and microfluidic channel.

Separation BGW-channel	3 μm	4 μm	5 μm	7 μm
Wavelength shift ($\pm 0.05\text{nm}$)	0.30	0.23	0.21	0.06

For the gap of 3 μm , we then filled the channel with water and were able to measure a different Bragg wavelength, figure 15.

The results obtained highlight one of the advantages of the FLICE technique: it can be used to integrate monolithically optical layers with microfluidic channels.

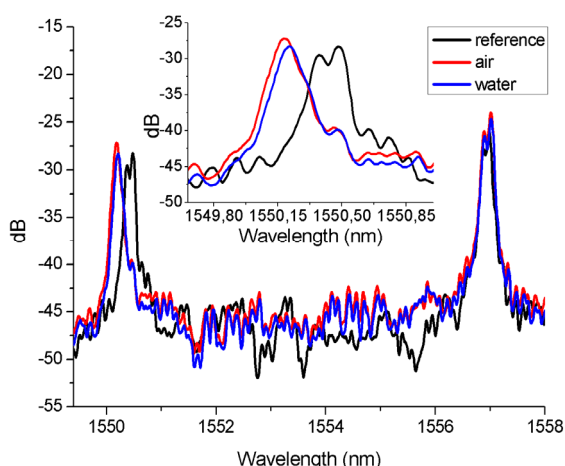


Figure 15: Optical spectrum of a BGW placed 3 μm from the microfluidic channel, when the channel is filled with air (red) and with water (blue). An initial spectrum (black), taken before the etching reaction, is also included. The inset picture shows that different Bragg wavelengths are obtained for air and water.

5 CONCLUSIONS

In this project, we employed the FLICE technique to study the fabrication process of microfluidic channels. From this study, we were able to produce centimetre long channels, with uniform aspect ratio and with crack-free and smooth sidewalls.

This optimization enabled monolithic integration of the channels with optical components. By producing Bragg grating waveguides a few microns from the microfluidic channels, we were able to detect the fluid through evanescent coupling.

These results, although preliminary, are important for the development of high-quality optofluidic devices.

ACKNOWLEDGEMENTS

Project "NanoSTIMA: Macro-to-Nano Human Sensing: Towards Integrated Multimodal Health Monitoring and Analytics/NORTE-01-0145-FEDER-000016" is financed by the North Portugal Regional Operational Programme (NORTE 2020), under the PORTUGAL 2020 Partnership Agreement, and through the European Regional Development Fund (ERDF).

REFERENCES

- Dittrich, P., Manz, A., 2006. Lab-on-a-chip: microfluidics in drug discovery. *Nature reviews. Drug discovery*, 5(3):210–218.
- Xu, B., Zhang, Y., Xia, H., Dong, W., Ding, H., Sun, H., 2013. Fabrication and multifunction integration of microfluidic chips by femtosecond laser direct writing. *Lab on a chip*, 13:1677–1690.
- Liu, K., Yang, Q., He, S., Chen, F., Zhao, Y., Fan, X., Li, L., Shan, C., Bian, H., 2013. A high-efficiency three-dimensional helical micromixer in fused silica. *Microsystem Technologies*, 19(7):1033–1040.
- Hwang, D., Kim, M., Hiromatsu, K., Jeon, H., Grigoropoulos, C., 2009. Three-dimensional optofluidic devices fabricated by ultrashort laser pulses for high throughput single cell detection and processing. *Applied Physics A: Materials Science and Processing*, 96(2):385–390.
- Vos, K., Bartolozzi, I., Schacht, E., Bienstman, P., Baets, R., 2007. Silicon-on-Insulator microring resonator for sensitive and label-free biosensing. *Optics Express*, 15(12):7610–7615.
- Wu, H., Wheeler, A., Zare, R., 2004. Chemical cytometry on a picoliterscale integrated microfluidic chip. *Proceedings of the National Academy of Sciences of the United States of America*, 101(35).
- Osellame, R., Cerullo, G., Ramponi, R., 2012. *Femtosecond Laser Micromachining*. Springer, 1st edition.
- Sugioka, K., Cheng, Y., 2014. *Femtosecond Laser 3D Micromachining for Microfluidic and Optofluidic Applications*, Springer, 1st edition.
- Corbari, C., Champion, A., Gecevicius, M., Beresna, M., Bellouard, Y., Kazansky, P., 2013. Femtosecond versus picosecond laser machining of nano-gratings and micro-channels in silica glass. *Optics Express*, 21(4).
- Zeil, P., Voigtländer, C., Thomas, J., Richter, D., Nolte, S., 2013. Femtosecond laser-induced apodized Bragg grating waveguides. *Optics Letters*, 38(13):2354–6.
- Davis, K., Miura, K., Sugimoto, N., Hirao, K., 1996. Writing waveguides in glass with a femtosecond laser. *Optics Letters*, 21(21):1729.
- Bellini, N., Vishnubhatla, K., Bragheri, F., Ferrara, L., Minzioni, P., Ramponi, R., Cristiani, I., Osellame, R., 2010. Femtosecond laser fabricated monolithic chip for optical trapping and stretching of single cells. *Optics Express*, 18(5):4679–4688.
- Applegate, R., Squier, J., Vestad, T., Oakey, J., Marr, D., Bado, P., Dugan, M., Said, A., 2006. Microfluidic sorting system based on optical waveguide integration and diode laser bar trapping. *Lab on a chip*, 6(3):422–426.
- Stone, H., Stroock, A., Ajdari, A., 2004. Engineering Flows in Small Devices: Microfluidics Toward a Lab-on-a-Chip. *Annual Review of Fluid Mechanics*, 36(1):381–411.
- Said, A., Dugan, M., Bado, P., Bellouard, Y., Scott, A., Mabesa, J., 2004. Manufacturing by laser direct-write

- of three-dimensional devices containing optical and microfluidic networks. *Proceedings of SPIE*, 5339:194–204.
- Taylor, R., Hnatovsky, C., Simova, E., 2008. Applications of femtosecond laser induced self-organized planar nanocracks inside fused silica glass. *Laser and Photonics Reviews*, 2(1-2):26–46.
- Champion, A., Beresna, M., Kazansky, P., Bellouard, Y., 2013. Stress distribution around femtosecond laser affected zones: effect of nanogratings orientation. *Optics express*, 21(21):24942–51.
- Agarwal, A., Tomozawa, M., 1997. Correlation of silica glass properties with the infrared spectra. *Journal of Non-Crystalline Solids*, 209(1-2):166–174.
- Kiyama, S., Matsuo, S., Hashimoto, S., Morihira, Y., 2009. Examination of etching agent and etching mechanism on femtosecond laser microfabrication of channels inside vitreous silica substrates. *Journal of Physical Chemistry C*, 113(27):11560–11566.
- Vishnubhatla, K., Bellini, N., Ramponi, R., Cerullo, G., Osellame, R., 2009. Shape control of microchannels fabricated in fused silica by femtosecond laser irradiation and chemical etching. *Optics Express*, 17(10):8685–8695.
- Ho, S., 2013. *Femtosecond Laser Microfabrication of Optofluidic Lab-on-a-Chip with Selective Chemical Etching*. PhD thesis, University of Toronto.

